Acta Mech 205, 77–84 (2009)
DOI 10.1007/s00707-009-0170-7

H. Hatami-Marbini · R. C. Picu

Effect of fiber orientation on the non-affine deformation of random fiber networks

Received: 16 September 2008 / Revised: 12 December 2008 / Published online: 4 April 2009

Abstract The study of fiber networks is essential in understanding the mechanical properties of many polymeric and biological materials. These systems deform non-affinely, i.e. the local deformation is different than the applied far-field. The degree of non-affinity increases with decreasing scale of observation. Here, we show that this relationship is a power law with a scaling exponent independent of the type of applied load. Preferential fiber orientation influences non-affinity in a significant way: this parameter generally increases upon increasing orientation. However, some components of non-affinity, such as that associated with the normal strain in the direction of the preferential fiber orientation, decrease. In random networks, the nature of the far-field has little influence on the level of non-affinity. This is not the case in oriented networks.

1 Introduction

The mechanics of random fiber networks is the key to understanding the complex response of biopolymer networks and gels to applied load. The cytoskeleton of eukaryotic cells is a network of filamentous proteins and cross-links [1]. Tissue templates [2], battery substrates [3] and paper [4,5] are among other examples where mechanics of fiber networks is important. The relation between the overall behavior of such networks and their microstructure is of interest.

The mechanical behavior of semiflexible networks is different from that of flexible networks. The strain energy is stored mainly entropically in flexible networks, while in semi-flexible networks it is stored enthalpically in the form of bending and extensional deformation of its constituents. This is because in semi-flexible networks, the persistence length is of the same order as the mean segment length. This is the case, for example, with F-actin fibers of cytoskeleton [6].

If the deformation field of a semiflexible network is assumed to be affine, i.e. the strain measured locally is identical to the far-field/applied strain, a closed-form relation for the overall response of the network in terms of fiber properties and orientation can be developed [7,8]. However, the deformation of random, cross-linked fiber networks is highly non-affine [9–12]. The energy level of a structure that deforms non-affinely is lower than that of the same structure undergoing affine deformation, so non-affine deformation at the microstructural level leads to more compliant response globally.

The validity of the affine assumption depends on the length scale of interest. The deformation is only affine at the scale of the entire system (by definition) and it becomes more non-affine as the scale of observation decreases [9,12]. Therefore, a proper understanding of non-affine deformation [13] is essential in the mechanics of these materials.

Various measures of non-affinity have been developed [9,12,14,15]. Since the behavior of random networks needs to be studied at various length scales, the probing length scale must be incorporated in the non-affinity

H. Hatami-Marbini (✉) · R. C. Picu
Department of Mechanical Aerospace and Nuclear Engineering, Rensselaer Polytechnic Institute, Troy, NY 12180, USA
E-mail: hatamh@rpi.edu

measure. Most current non-affinity measures cannot be easily related to mechanical fields or to a tangible property of the network. Recently we defined a measure based on the gradients of the displacement field [12]. The probing length scale is incorporated into this strain-based measure. The measure provides a unified description of non-affinity in both strain and rotation. Here, we use the same non-affinity measure to study the influence of the far-field loading and of preferential fiber orientation on the degree of non-affinity of the network deformation.

2 Problem statement

Two-dimensional random fiber networks produced by depositing fibers in a square domain of size L are considered. The initial orientation of fibers is random or selected according to a specified distribution function, in separate models. All fibers in the model have the same length, L_0. Fibers are assumed to be connected rigidly at the crossing points and to be made from the same material (identical bending stiffness κ and axial stiffness η). Many dangling ends are produced during fiber deposition; their influence on deformation is neglected as excluded volume effects are not considered in this model. As the network is grown, rigidity percolation is reached at a critical point defined by a critical fiber number density [10]. This threshold depends on fiber orientation.

There are four characteristic lengths in a random fiber network, the system size, L, the fiber length, L_0, the mean segment length, l_c and a parameter with units of length representing the relative importance of fiber bending and axial stiffness (κ and η, respectively), $l_b = \sqrt{\kappa/\eta}$. The mean segment length is related directly to the fiber number density, N, as $l_c \sim \pi/2NL_0$, for large N [16]. We studied the effect of these characteristic lengths on the non-affine behavior of random fiber networks [12]. Here we provide new data on the influence of the far-field loading type and fiber initial orientations on the network non-affinity. For this purpose, the system is subjected to displacement-imposed (small strains) uniaxial, biaxial and shear deformation. The solution is obtained via energy minimization using a finite element solver or the conjugate gradient method. The total energy is computed as the sum of strain energies associated with bending and axial deformation of fibers over the entire system.

3 Strain-based non-affinity measure

The measure of non-affinity used in this work is similar to that introduced in [12] and is based on the fluctuation of the actual strain/rotation relative to the respective affine quantity (or the far-field). If at length scale r, the strain field $\boldsymbol{\varepsilon} = (\varepsilon_{11}, \varepsilon_{22}, \varepsilon_{12})$ and the rotation ω_{12} are known, the non-affinity is defined as the fluctuation of $\boldsymbol{\varepsilon}$ and ω_{12} relative to the respective affine estimates:

$$\mathbf{H}(r) = (H_1, H_2, H_3, H_4) = \left\langle \left(\boldsymbol{\Xi} - \boldsymbol{\Xi}^{\mathrm{aff}} \right)^2 \right\rangle_r , \tag{1}$$

where $\boldsymbol{\Xi} = (\varepsilon_{11}, \varepsilon_{22}, \varepsilon_{12}, \omega_{12})$. The operator $\langle\ \rangle$ stands for averaging over the entire problem domain and the index r denotes the length scale on which $\mathbf{H}$ is computed. It should be mentioned that $\mathbf{H}$ does not have tensorial properties.

The gradient of the displacement field, $\partial u_i/\partial x_j$, $i, j = 1, 2$ and subsequently components of $\boldsymbol{\Xi}$ are calculated on various length scales as follows: once the nodal displacements are obtained, a triplet of network nodes is chosen such that they form approximately an equilateral triangle. The displacement field within the triangle is written in terms of nodal displacements ($\mathbf{u}^i$, $i = 1, \ldots, 3$) using interpolation functions of the constant-strain triangular (CST) element from the finite element method:

$$\begin{aligned} u_1(x_1, x_2) &= N_i(x_1, x_2) u_1^i, \\ u_2(x_1, x_2) &= N_i(x_1, x_2) u_2^i. \end{aligned} \tag{2}$$

The shape functions of the CST element are:

$$\begin{aligned} N_1(x_1, x_2) &= \frac{1}{2A}\left(\left(x_1^2 x_2^3 - x_1^3 x_2^2\right) + \left(x_2^2 - x_2^3\right) x_1 + \left(x_1^3 - x_1^2\right) x_2 \right), \\ N_2(x_1, x_2) &= \frac{1}{2A}\left(\left(x_1^3 x_2^1 - x_1^1 x_2^3\right) + \left(x_2^3 - x_2^1\right) x_1 + \left(x_1^1 - x_1^3\right) x_2 \right), \\ N_3(x_1, x_2) &= \frac{1}{2A}\left(\left(x_1^1 x_2^2 - x_1^2 x_2^1\right) + \left(x_2^1 - x_2^2\right) x_1 + \left(x_1^2 - x_1^1\right) x_2 \right), \end{aligned} \tag{3}$$

where A is the area of the triangle and x_1^i and x_2^i are the Cartesian coordinates of node i with respect to a global coordinate system. The constant strain field $\boldsymbol{\varepsilon} = (\varepsilon_{11}, \varepsilon_{22}, \varepsilon_{12})$ and the rotation ω_{12} associated to each triplet of nodes can be evaluated from the gradient of the displacement, Eq. (2), using the small strain definition, i.e. $\varepsilon_{ij} = (\partial u_i/\partial x_j + \partial u_j/\partial x_i)/2$ for $i, j = 1, 2$ and $\omega_{12} = (\partial u_1/\partial x_2 - \partial u_2/\partial x_1)/2$. If the length of each edge of a given triangle is a, the resulting gradients are considered to be the average of the underlying field over the length scale $r = \sqrt{A} = (3^{1/4}/2)a$. The mean of these quantity over the entire system is equal to the affine strain (imposed far-field), $\boldsymbol{\varepsilon}^{\text{aff}}$, i.e. $\langle \varepsilon_{ij} \rangle_r = \varepsilon_{ij}^{\text{aff}}$, for any r.

This non-affinity measure, Eq. (1), is independent of the far-field loading and separates the strain and rotation components. Moreover, since it is based on strain, it facilitates direct comparison with fields predicted using continuum models of the discrete structure.

4 Results

In this work, we study the effect of fiber orientations and type of loading on the non-affine behavior of random fiber networks. In what follows, the non-affinity measure is normalized with the value of the far-field ($\overline{\mathbf{H}} = \mathbf{H}/\varepsilon_0^2$), while the probing length scale r is normalized with the fiber length, L_0. In all models, the fiber number density N is chosen such that the network is significantly above the percolation threshold and l_b/L_0 is kept constant, $l_b/L_0 = 10^{-4}$. A discussion of the effect of l_b and N on the field fluctuations can be found in [12]. Unless otherwise stated, the following results are obtained from averaging over 10–15 realizations of the network.

4.1 Effect of far-field loading on non-affinity

Let us consider first randomly oriented fiber networks with same fiber number density, $N = 200$, subjected to a uniform uniaxial strain $\boldsymbol{\varepsilon} = (\varepsilon_0, 0, 0)$ and to a simple shear $\varepsilon = (0, \varepsilon_0, 0)$, in separate simulations. Figure 1 shows components of the normalized non-affinity measure, Eq. (1), versus the probing length scale. Few interesting observations can be made. For a given system, all components of $\mathbf{H}$ are of the same magnitude and scale as a power law of the scale of observation, r. The rotation component (H_4) is of similar magnitude as the other components of $\mathbf{H}$. The non-affinity in the rotation ω_{12} relates to multiple observations of rotatory structures in the non-affine displacements of granular materials [17]. The scaling exponent is identical for all components of $\mathbf{H}(1.60 \pm 0.05)$. These conclusions were obtained also in [12] for a different system. The non-affinity appears to depend weakly on the applied far-field, with the curves corresponding to uniaxial and shear loading almost overlapping. In [12], it is shown that the power law behavior of the non-affinity measure is independent of the fiber number density.

Head et al. [9,16] measured the non-affinity as the fluctuation of the angle θ of a vector connecting two structural nodes (fiber crossings) relative to the rotation angle θ resulting from an affine deformation, θ^{aff}. This quantity is evaluated as an ensemble average over vectors of length r:

$$\delta\theta^2(r) = \left\langle \left(\theta - \theta^{\text{aff}}\right)^2 \right\rangle_r , \tag{4}$$

We refer to this measure as the θ-measure of non-affinity. Figure 2 compares the θ-measure with the strain-based measure defined here (Eq. 1) for a network with fiber density $N = 400$ subjected to various types of loadings. It is seen that both measures give the same qualitative behavior but the scaling exponents are not identical. As mentioned above, the type of far-field load applied has a weak influence on both measures.

Although the non-affinity decreases fast with increasing the scale of observation, in a system with system size L larger than any other material length scale, it does not vanish identically. The power law scaling in Figs. 1 and 2 indicates that the system has no characteristic length scale that separates affine from non-affine mechanical response. Therefore, any affine model can be only an approximation of the actual network response.

4.2 Effect of initial fiber orientation and length distributions on non-affinity

In order to study the effect of preferential fiber orientation in the undeformed network, systems with fibers of same length L_0 are produced by sampling a double peaked Gaussian distribution, with maxima at both 0°

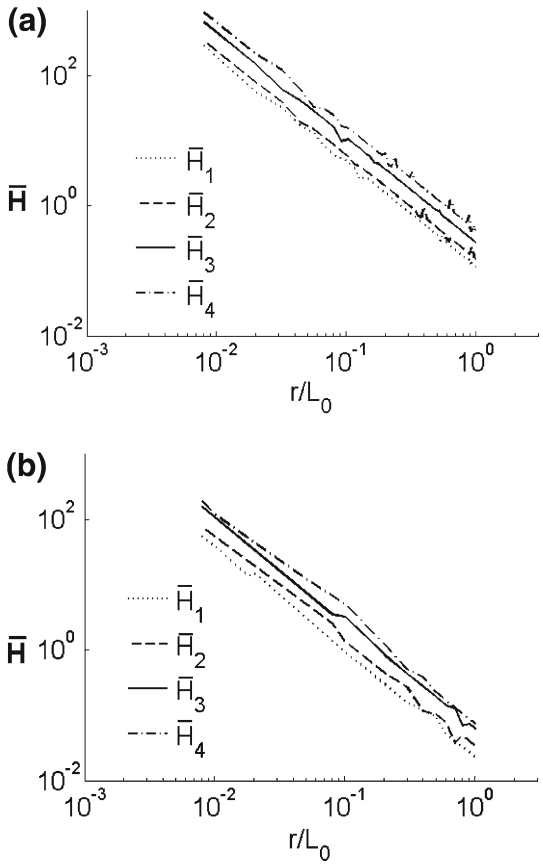

Fig. 1 Normalized non-affinity measure $\overline{\mathbf{H}}(r) = \mathbf{H}(r)/\varepsilon_0^2$ against the normalized probing length scale, r/L_0, for a network of density $N = 200$ fibers per unit area and $l_b/L_0 = 10^{-4}$ subjected to the (**a**) uniaxial far-field strain $\boldsymbol{\varepsilon} = (\varepsilon_0, 0, 0)$ and (**b**) shear far-field strain $\boldsymbol{\varepsilon} = (0, 0, \varepsilon_0)$

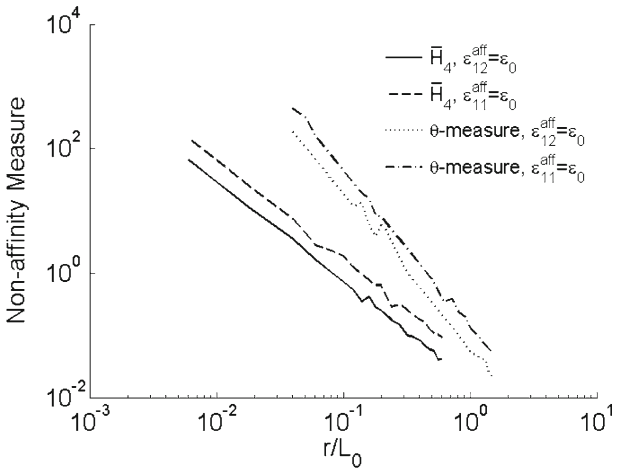

Fig. 2 Comparison of component $\overline{H}_4 = H_4/\varepsilon_0^2$ of the normalized non-affinity measure of Eq. (1) with the θ-measure of Eq. (4) [9,16]. Both measures are computed from the same system of density $N = 400$ fibers per unit area and $l_b/L_0 = 10^{-4}$. Both uniaxial and shear far-fields were applied. The two measures capture the same qualitative behavior, but with different scaling exponents

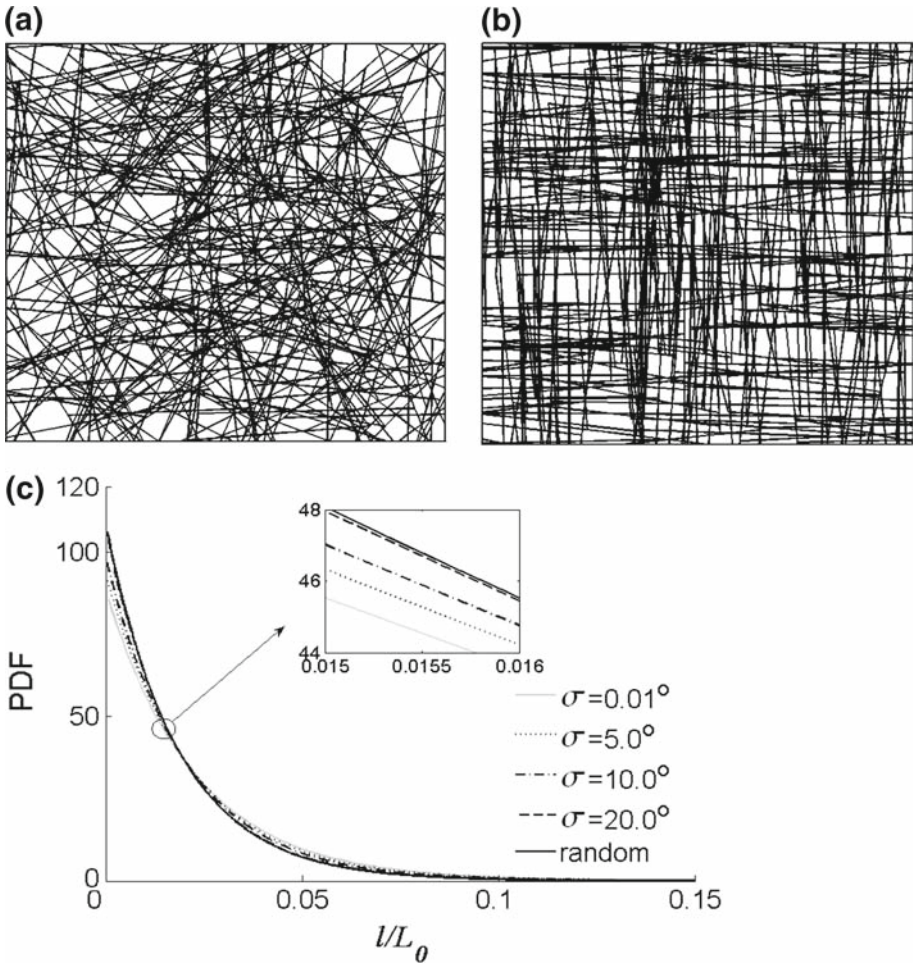

Fig. 3 Realizations of networks with (**a**) random and (**b**) preferential fiber orientation and fiber number density $N = 400$. In **b**, the orientation is chosen from a bimodal distribution having two Gaussian peaks centered at 0° and 90°, both having 5° standard deviation (σ). (**c**) Probability distribution function (PDF) of the segment length, l, for several realizations of the type shown in **b** and with various standard deviations of the two Gaussian peaks. The *inset* shows a detail of the curves

and 90° relative to the x_1 axis. The results are compared with similar data obtained from models with uniform distribution (random fiber orientation) and shown in Fig. 1. The objective is to determine to what extent the fiber orientation influences non-affinity (and hence the departure from predictions of stiffness based on affine models). Figures 3a and b shows two realizations of networks with random orientation and with orientation sampled from the bimodal distribution with standard deviation $\sigma = 5°$.

Before proceeding, it is important to determine whether all characteristic lengths defined in Sect. 2 are identical in the two systems shown in Fig. 3. In fact, since N and L_0 are identical, the only parameter that may differ is the segment length distribution l and its mean, l_c. Figure 3c shows the probability distribution function of l for the random and preferential orientations corresponding to different values of the parameter σ. The curves are almost identical. Likewise, l_c in these various systems is essentially identical. This insures that the effects discussed below are due entirely to the preferential orientation of fibers. It should be noted that for values of the standard deviation, σ equal or larger than 20°, the realizations are visually indistinguishable from the network with random fiber orientations.

The first finding is shown in Fig. 4 which represents the scaling of the non-affinity measure $\overline{\mathbf{H}}(r) = \mathbf{H}(r)/\varepsilon_0^2$ for the oriented network in Fig. 3b (with $N = 400$ and $l_b/L_0 = 10^{-4}$) subjected to far-field uniaxial strain $\boldsymbol{\varepsilon} = (\varepsilon_0, 0, 0)$. As in the case of the random network, all components of $\overline{\mathbf{H}}$ scale in the same manner and have approximately the same magnitude. The exception is $\overline{H}_2$ which is smaller than the other components of $\overline{\mathbf{H}}$. The behavior is more affine in this direction because the Poisson effect is very small due to the special geometry of the network. The fibers are distributed mostly perpendicular and in the direction of applied far-field

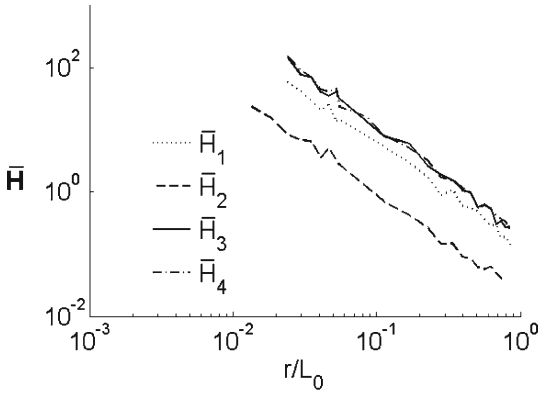

Fig. 4 Normalized non-affinity measure $\overline{\mathbf{H}}(r) = \mathbf{H}(r)/\varepsilon_0^2$ against the normalized probing length scale, r/L_0, for the preferential oriented network in Fig. 3b subjected to the uniform far-field uniaxial strain $\boldsymbol{\varepsilon} = (\varepsilon_0, 0, 0)$. The non-affinity in the normal strain in the direction normal to the loading direction, $\overline{H}_2$, is smaller than non-affinity in other directions

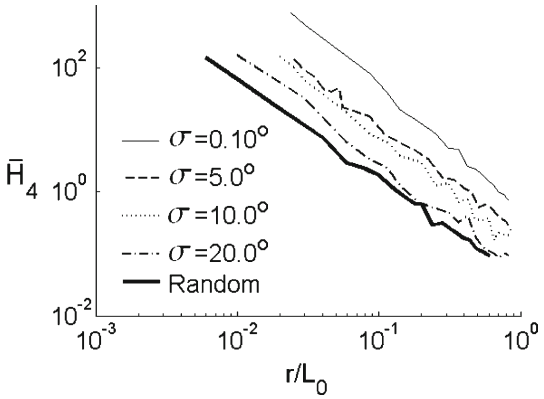

Fig. 5 Component $\overline{H}_4 = H_4/\varepsilon_0^2$ of the normalized non-affinity measure versus the normalized probing length scale, r/L_0, for preferentially oriented systems with the same fiber number density ($N = 400$) and $l_b/L_0 = 10^{-4}$ subjected to uniform far-field uniaxial strain $\boldsymbol{\varepsilon} = (\varepsilon_0, 0, 0)$. The fiber orientation is defined by a bimodal probability distribution function with Gaussian peaks at 0° and 90° and with various standard deviations, σ. The random orientation case is shown for reference

strain; therefore, the amount of load supported by fibers oriented normal to the loading direction and hence the non-affinity in this direction is negligible.

Let us now compare the values of $\overline{\mathbf{H}}$ in random and preferentially oriented networks having identical characteristic lengths. We consider systems with $N = 400$ fibers per unit area and $l_b/L_0 = 10^{-4}$ subjected to $\boldsymbol{\varepsilon} = (\varepsilon_0, 0, 0)$. Figure 5 shows $\overline{H}_4$ for systems similar to those in Fig. 3 and with various σ's. As above, all these systems have identical distribution of segment lengths (Fig. 3c). It is seen that the non-affinity decreases as the randomness of fiber orientation increases. This behavior is associated with the stability of the network. As the networks become more and more oriented (biaxially), a soft deformation mode develops in shear. This is related to the elevated sensitivity of $\overline{H}_4$ to orientation seen in Fig. 5.

It is instructive to consider next networks preferentially oriented in one direction only. To this end, the initial orientation of fibers is chosen from a Gaussian distribution function centered on 0° relative to the x_1 axis and with standard deviation $\sigma = 10°$. A detail of the resulting geometry is shown in the inset of Fig. 6. The system has $N = 800$ fibers per unit area, $l_b/L_0 = 10^{-4}$ and is subjected to far-field uniaxial strain $\boldsymbol{\varepsilon} = (\varepsilon_0, 0, 0)$. The non-affinity is shown in Fig. 6. The component $\overline{H}_1$ is much smaller than the others. This more affine response in the direction of the preferential orientation of fibers is expected since in the limit, when all fibers are perfectly aligned in the stretch direction, the non-affinity in the respective direction should decrease to zero.

Moreover, let us consider the system of Fig. 6 which is now loaded uniaxially in the direction perpendicular to the direction of preferential fiber orientation, $\boldsymbol{\varepsilon} = (0, \varepsilon_0, 0)$. Figure 7 shows a comparison of the non-affinity in this system when loaded along and perpendicular to the fiber orientation. It is first observed that the type of

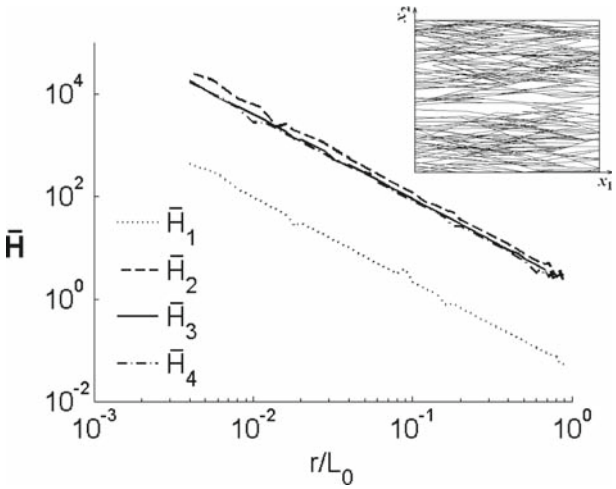

Fig. 6 Normalized non-affinity measure $\overline{\mathbf{H}}(r) = \mathbf{H}(r)/\varepsilon_0^2$ against the normalized probing length scale, r/L_0, for the preferentially oriented network in the *inset*, with density $N = 800$ fibers per unit area and $l_b/L_0 = 10^{-4}$, subjected to uniaxial far-field strain $\boldsymbol{\varepsilon} = (\varepsilon_0, 0, 0)$. The fiber initial orientation follows a normal distribution with mean zero and standard deviation of 10° from the direction of the applied strain, x_1. The non-affinity in the direction of the preferential orientation is significantly smaller than in all other components of $\overline{\mathbf{H}}$

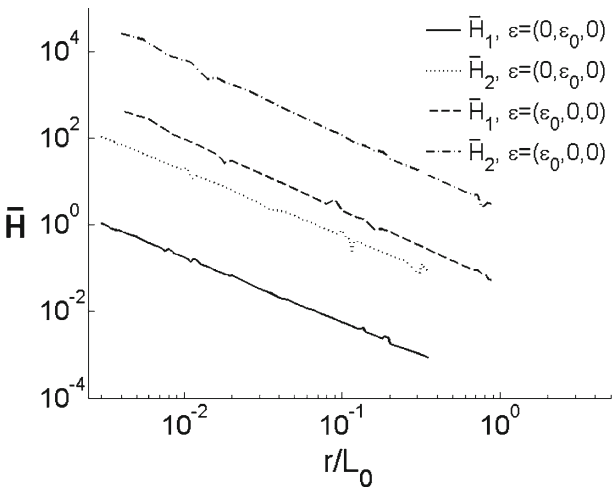

Fig. 7 Components of the non-affinity measure $\overline{\mathbf{H}}(r) = \mathbf{H}(r)/\varepsilon_0^2$ against the normalized probing length scale, r/L_0, for the network in Fig. 6 loaded in direction x_2, perpendicular to the preferential fiber orientation, $\boldsymbol{\varepsilon} = (0, \varepsilon_0, 0)$. Data from Fig. 6 are added for reference. The non-affinity is significantly smaller when the loading is perpendicular to the fiber orientation. The smallest non-affinity is always measured in the preferential direction

loading does make a difference in these anisotropic systems. Furthermore, the non-affinity is always smaller in the direction of preferential fiber orientation, irrespective of how the network is loaded.

5 Conclusion

The mechanics of random fiber networks above the rigidity percolation threshold is non-affine at all scales. As the scale of observation decreases, the non-affinity increases following a power law scaling with exponent of 1.60 ± 0.05 (for the networks considered here). Fiber orientation plays an important role. Randomly oriented networks deform more affinely than preferentially oriented networks. The type of far-field loading has no effect on the degree of non-affinity as long as the network is randomly oriented, but becomes important when fibers are preferentially oriented.

References

1. Janmey, P.A.: Mechanical properties of cytoskeletal polymers. Curr. Opin. Cell Biol. **4**, 4–11 (1991)
2. Chandran, P.L., Barocas, V.H.: Affine versus non-affine fibril kinematics in collagen networks: theoretical studies of network behavior. J. Biomech. Eng. **128**, 259–270 (2006)
3. Wang, C.W., Cheng, X., Sastry, A.M., Choi, S.B.: Investigation of failure processes in porous battery substrates. Part I. Experimental findings. J. Eng. Mater. Technol. **121**, 503–513 (1999)
4. Alava, M., Niskanen, K.: The physics of paper. Rep. Prog. Phys. **69**, 669–723 (2006)
5. Ostoja-Starzewski, M., Stahl, D.C.: Random fiber networks and special elastic orthotropy of paper. J. Elast. **60**, 131–149 (2000)
6. Kroy, K., Frey, E.: Force–extension relation and plateau modulus for wormlike chains. Phys. Rev. Lett. **77**, 306–39 (1996)
7. Wu, X.F., Dzenis, Y.A.: Elasticity of planar fiber networks. J. Appl. Phys. **98**, 093501 (2005)
8. Narter, M.A., Barta, S.K., Buchanan, D.R.: Micromechanics of three-dimensional fiberwebs: constitutive equations. Proc. R. Soc. A **455**, 3543–3563 (1998)
9. Head, D.A., Levine, A.J., MacKintosh, F.C.: Distinct regimes of elastic response and deformation modes of cross-linked cytoskeletal and semiflexible polymer networks. Phys. Rev. E **68**, 061907 (2003)
10. Wilhelm, J., Frey, E.: Elasticity of stiff polymer networks. Phys. Rev. Lett. **91**, 108103 (2003)
11. Onck, P.R., Koeman, T., van Dillen, T., vand der Giessen, E.: Alternative explanation of stiffening in cross-linked semiflexible networks. Phys. Rev. Lett. **95**, 178102 (2005)
12. Hatami-Marbini, H., Picu, R.C.: Scaling of nonaffine deformation in random semiflexible fiber networks. Phys. Rev. E **77**, 062103 (2008)
13. Heussinger, C., Frey, E.: Stiff polymers, foams, and fiber networks. Phys. Rev. Lett. **96**, 017802 (2006)
14. DiDonna, B.A., Lubensky, T.C.: Nonaffine correlations in random elastic media. Phys. Rev. E **72**, 066619 (2005)
15. Langer, S.A., Liu, A.J.: Nonaffine correlations in random elastic media. J. Phys. Chem. B **101**, 8667–8671 (1997)
16. Head, D.A., MacKintosh, F.C., Levine, A.J.: Nonuniversality of elastic exponents in random bond-bending networks. Phys. Rev. E **68**, 025101 (2003)
17. Leonforte, F., Tanguy, A., Wittmer, J.P., Barrat, J.L.: Continuum limit of amorphous elastic bodies. II. Linear response to a point source force. Phys. Rev. B **70**, 014203 (2004)